Earth and Planetary Science Letters 512 (2019) 1–7

Contents lists available at ScienceDirect

Earth and Planetary Science Letters

www.elsevier.com/locate/epsl

Timing and structure of Termination II in north China constrained by a precisely dated stalagmite record

Wuhui Duan [a,b,c,*], Hai Cheng [d,e], Ming Tan [a,**], Xianglei Li [d], R. Lawrence Edwards [e]

[a] Key Laboratory of Cenozoic Geology and Environment, Institute of Geology and Geophysics, Chinese Academy of Sciences, Beijing 100029, China
[b] CAS Center for Excellence in Life and Paleoenvironment, Beijing 100044, China
[c] Connected Waters Initiative Research Centre, University of New South Wales, Sydney 2052, Australia
[d] Institute of Global Environmental Change, Xi'an Jiaotong University, Xi'an 710049, China
[e] Department of Earth Sciences, University of Minnesota, Minneapolis, MN 55455, USA

ARTICLE INFO

Article history:
Received 3 April 2018
Received in revised form 2 January 2019
Accepted 24 January 2019
Available online 12 February 2019
Editor: J. Adkins

Keywords:
Termination II
north China
speleothem record
timing and structure

ABSTRACT

The timing and structure of Termination II (T-II) is still debatable as the number of high-quality records is insufficient. This study presents precisely dated stalagmite $\delta^{18}O$ data between 133.4 ± 0.3 to 126.6 ± 0.3 ka BP (covering most of T-II) from north China, near the northern limit of the East Asian summer monsoon (EASM), an area sensitive to climate change. The onset of the last interglacial is constrained at 129.4 ± 0.3 ka BP, consistent with south Chinese speleothem records, further supporting the idea that Northern Hemisphere summer insolation plays an important role in initiating glacial terminations. An extended interval of heavy $\delta^{18}O$ is observed immediately prior to this abrupt transition, named as the "Weak Monsoon Interval" (WMI) in south Chinese cave records, which was associated with the Heinrich Stadial 11 (H11) in the North Atlantic. A significant millennial-scale interstadial peaking at 132.7 ± 0.3 ka BP is identified preceding the weakest phase of the WMI. A synchronous counterpart is also found in some south Chinese speleothem and North Atlantic alkenone Mg/Ca SST records. It is inferred that the main H11 freshwater penetration possibly occurred after 131.5 ka BP, leaving some aspects of ocean and atmospheric circulation still in interstadial mode from 134 to 131.5 ka BP. Following the onset of the last interglacial, there was a millennial-scale "pause" in our $\delta^{18}O$ record, synchronized with a "slowdown" in the rate of decrease in $\delta^{18}O$ in south Chinese cave records. This is possibly a large regional climate oscillation, as it is also identified in some North Atlantic records, but one which is too weak to be a Younger Dryas (YD)-type event.

In summary, compared to south Chinese cave records, significant millennial-scale climate oscillations before and after the synchronous onset of the last interglacial is the main feature of our record. Nevertheless, the sequence of these climate events remains very different from Termination I (T-I), which is possibly ascribed to the stronger insolation, higher atmosphere CO_2, and the resultant faster and greater meltwater pulse to the North Atlantic during T-II than during T-I.

1. Introduction

Investigations of the sequence of climate events surrounding glacial terminations are important to address the issues associated with rapid climate change such as global warming. To uncover the underlying dynamics responsible for the glacial–interglacial transition, the last two deglaciations have been studied using marine records (Grant et al., 2012; Martrat et al., 2014; Tzedakis et al., 2018), Antarctic ice-core records (Petit et al., 1999) and speleothem records (Bar-Matthews et al., 2003; Cheng et al., 2006, 2009; Wang et al., 2008, 2018). Nevertheless, the penultimate deglaciation (Termination II, T-II) is still enigmatic, compared to the extensively studied last deglaciation (Termination I, T-I) as the number of high-quality records is insufficient.

It is undisputed that T-I was abruptly interrupted by a millennial-scale cold spell, the Younger Dryas (YD), a reversal to near-glacial conditions. In contrast, it is unclear whether there was also a YD-type event during T-II. While some records show no evidence of such an extreme climate reversal, a "climate pause" is

* Corresponding author at: Key Laboratory of Cenozoic Geology and Environment, Institute of Geology and Geophysics, Chinese Academy of Sciences, Beijing 100029, China.
** Corresponding author.
E-mail addresses: duanwuhui@mail.iggcas.ac.cn (W. Duan), tanming@mail.iggcas.ac.cn (M. Tan).

https://doi.org/10.1016/j.epsl.2019.01.043
0012-821X/

identified in marine records from the Iberian margin, the Mediterranean Sea (Grant et al., 2012; Jiménez-Amat and Zahn, 2015; Marino et al., 2015; Tzedakis et al., 2018), and the central Nordic Sea (Bauch et al., 2012), as well as in a few European speleothem records (Drysdale et al., 2009; Grant et al., 2012; Moseley et al., 2015; Tzedakis et al., 2018), though the timing, structure and magnitude of this event varies.

The oxygen isotope records of speleothems from south China in the East Asian summer monsoon (EASM) region show a two-step evolution during the last two deglaciations: (1) a "Weak Monsoon Interval" (WMI) corresponding to a Heinrich stadial and, (2) the abrupt transition from the WMI to the interglacial (Cheng et al., 2006, 2009; Kelly et al., 2006). The WMI of T-I is split into two WMIs, the Heinrich stadial 1 (H1) and the YD, by an interstadial, the Bølling-Allerød (BA) (Wang et al., 2001), whereas the WMI of T-II is only interrupted by an inconspicuous interstadial in Sanbao and Dongge cave records (Cheng et al., 2009; Kelly et al., 2006), and is divided into two WMIs by an interstadial with high amplitude and short duration in Hulu records (Cheng et al., 2006; Wang et al., 2018). The two WMIs in Hulu records are possibly correlated with the cold events contained in Heinrich stadial 11 (H11) (Tzedakis et al., 2018). In any case, the WMI of T-II is only corresponding to the H11 but not including a YD-type event (Cheng et al., 2006, 2009; Kelly et al., 2006). Nevertheless, there is an interval of "slowdown" in the decline rates of $\delta^{18}O$ values immediately after the last interglacial onset in both the Dongge and Sanbao records, which was suggested to be associated with the "T-II pause" in European records (Moseley et al., 2015). This relation, however, should be further confirmed by the records in higher latitude, such as north China.

Located near the northern limit of the EASM, north China lies in the transitional zone between the cold air masses from high-latitude polar regions and the warm-moist air masses originating from low-latitude seas. Therefore, precipitation in north China is much more sensitive to the fluctuations of EASM than in south China, and rainfall in north China is a reliable indicator of EASM intensity. Stronger (weaker) EASM circulation carries more (less) water vapor from the tropical Pacific and Indian Oceans, and results in the higher (lower) precipitation over north China (Liu et al., 2014). Some stalagmite records from north China document the centennial- and decadal-scale climate oscillations recorded in Greenland ice cores during the last glacial period (Duan et al., 2016a; Ma et al., 2012), while speleothem records from south China show a less clear picture (Dykoski et al., 2005; Liu et al., 2010; Wang et al., 2001). Thus, well-dated, high-resolution speleothem records covering T-II from north China have the potential to reduce the uncertainties in the relationship between low- and high-latitude records during the penultimate deglaciation. Here, we present a precisely dated stable isotope record from Xinglong Cave, which depicts the precise timing and detailed structure of T-II in north China for the first time, helping to refine the nature of T-II.

2. Cave and setting

Xinglong Cave (40°29′N, 117°29′E, 710 m a.s.l.) is located in Hebei Province, north China, close to the northern boundary of the EASM (Supplementary materials, Fig. S1). The local mean annual temperature and precipitation are 9.1°C and 512 mm, respectively, with cold/dry winters and warm/wet summers and ~68% of the total annual precipitation falling during summer (June to August) (AD 1971–2000). The relative humidity in the cave ranges from 95 to 100% throughout most of the year (Duan et al., 2016a).

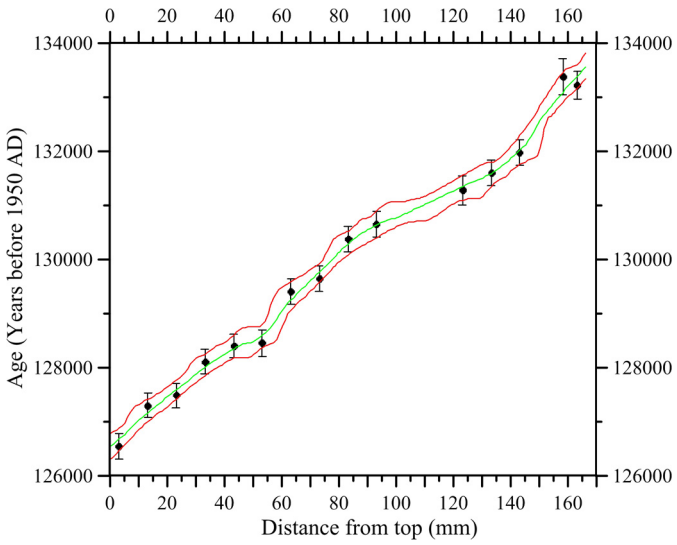

Fig. 1. Age-depth plot for stalagmite XL-4. The ^{230}Th age model was established using the StalAge algorithm (Scholz and Hoffmann, 2011). The green line indicates the derived age model and the red lines represent the 95% uncertainty envelopes. Error bars indicate 2σ uncertainties. (For interpretation of the colors in the figure(s), the reader is referred to the web version of this article.)

3. Sample and methods

A stalagmite sample (XL-4), 170 mm in length, was found already broken in the middle part of a collapse slope in the cave, approximately 17 m above the floor of the cave. It has a 'candlestick' shape and is 10 cm wide (Fig. S2), indicating rather stable growth conditions (Baker et al., 2007).

15 sub-samples for ^{230}Th dating analyses were drilled with a 0.9-mm diameter carbide dental burr along the stalagmite growth axis and analyzed on a multi-collector inductively coupled plasma mass spectrometer (Thermo Fisher NEPTUNE PLUS). The procedures are similar to those described in Cheng et al. (2013). The chemical procedures used to separate uranium and thorium followed those described in Edwards et al. (1987). For stable isotopic measurements, 174 powder samples were drilled along the growth axis with a 0.3-mm diameter carbide dental burr. The spatial resolution varies from 0.5 to 1 mm, corresponding to an average temporal resolution of 38 yr. An additional 28 sub-samples were drilled along individual growth layer for the Hendy test (Hendy, 1971). Analyses were performed on a Finnigan MAT-253 mass spectrometer equipped with a Kiel Carbonate Device IV. Interlaboratory standard TTB1 was run every 10–15 samples. All oxygen isotope values are reported relative to the Vienna Pee Dee Belemnite (VPDB) standard. Precision of the $\delta^{18}O$ analyses was better than 0.15‰ (2σ).

Both the ^{230}Th dating and oxygen isotopic measurements were performed in the Isotope Laboratory of Xi'an Jiaotong University.

4. Results

4.1. Chronology

15 high-precision ^{230}Th dates show that stalagmite XL-4 grew continuously from 133.4 ± 0.3 to 126.6 ± 0.3 ka BP (Supplementary materials, Table S1), covering the latter portion of the penultimate glacial period and the subsequent transition into the last interglacial. All dates are in stratigraphic order within errors (2σ), ranging from 222 to 330 yr (Table S1). The age model was constructed using the StalAge Monte-Carlo simulation, and the 95% confidence limit was calculated from the distribution of the simulated fits (Scholz and Hoffmann, 2011) (Fig. 1).

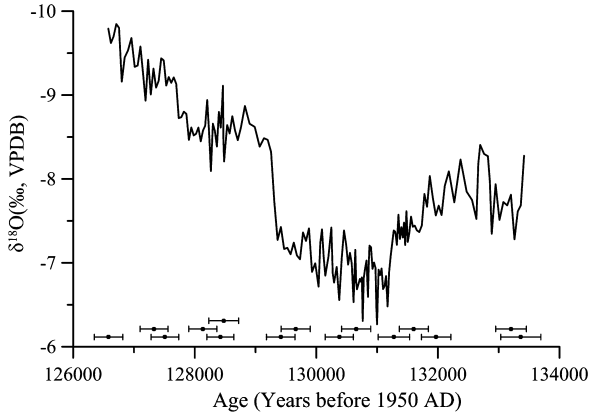

Fig. 2. $\delta^{18}O$ profile of stalagmite XL-4 based on the age model of the StalAge algorithm (Scholz and Hoffmann, 2011). ^{230}Th dating errors (2σ) are indicated at the bottom.

4.2. $\delta^{18}O$ profile

The XL-4 $\delta^{18}O$ fluctuates dramatically throughout the whole profile, varying between −9.85‰ and −6.27‰, with an average of −7.87‰ (Fig. 2 and Table S2). Two phases are separated by an abrupt negative shift in $\delta^{18}O$ at around 129.4 ± 0.3 ka BP. During the first phase (133.4 ± 0.3 to 129.4 ± 0.3 ka BP), $\delta^{18}O$ is relatively positive and shows a pronounced millennial-scale negative excursion, while during the second phase (129.4 ± 0.3 to 126.6 ± 0.3 ka BP), $\delta^{18}O$ displays a step-wise decrease from −7.3‰ to −9.8‰ with an abrupt transition and a small oscillation (Fig. 2).

5. Discussion

5.1. The climate interpretation of the XL-4 $\delta^{18}O$ signal

To assess whether the XL-4 $\delta^{18}O$ can be interpreted as a climate proxy, Hendy tests (Hendy, 1971) were performed. Along a specific growth layer, $\delta^{18}O$ values are essentially the same (Fig. S3a), with no statistically significant correlation between $\delta^{18}O$ and $\delta^{13}C$ (Fig. S3b), suggesting that the stalagmite most likely grew close to isotopic equilibrium. This is consistent with the stalagmite morphology (Baker et al., 2007). Thus, variations of the XL-4 $\delta^{18}O$ mainly reflect the recharging drip water $\delta^{18}O$ and the cave temperature. The temperature-dependent fractionation between calcite and water is too small (−0.23‰/°C) (Friedman and O'Neil, 1977) to cause the large amplitude of this record (3.58‰), suggesting that the primary control on the stalagmite $\delta^{18}O$ value is the oxygen isotope composition of drip water rather than the cave temperature. In turn, drip water $\delta^{18}O$ in north China, in most cases, is close to the weighted average oxygen isotope composition of local meteoric precipitation (Duan et al., 2016b).

Because of the high similarity in the millennial-scale events between Chinese speleothems and Greenland ice-core records, the major shifts in Chinese stalagmite $\delta^{18}O$ values are generally considered as an indicator of seasonal monsoon change, with lower $\delta^{18}O$ values reflecting a stronger EASM and vice versa (Cheng et al., 2006; Wang et al., 2001). Nevertheless, the interpretation of Chinese stalagmite $\delta^{18}O$ records remains highly controversial since they might be affected by various factors such as moisture sources (Clemens et al., 2010), vapor transport path (Pausata et al., 2011) and circulation patterns (Tan, 2014). Recently, a model-data comparison argued that Chinese speleothem $\delta^{18}O$ is a robust indicator of the EASM intensity but expressed as the southerly monsoon winds and rainfall amount in north China (Liu et al., 2014).

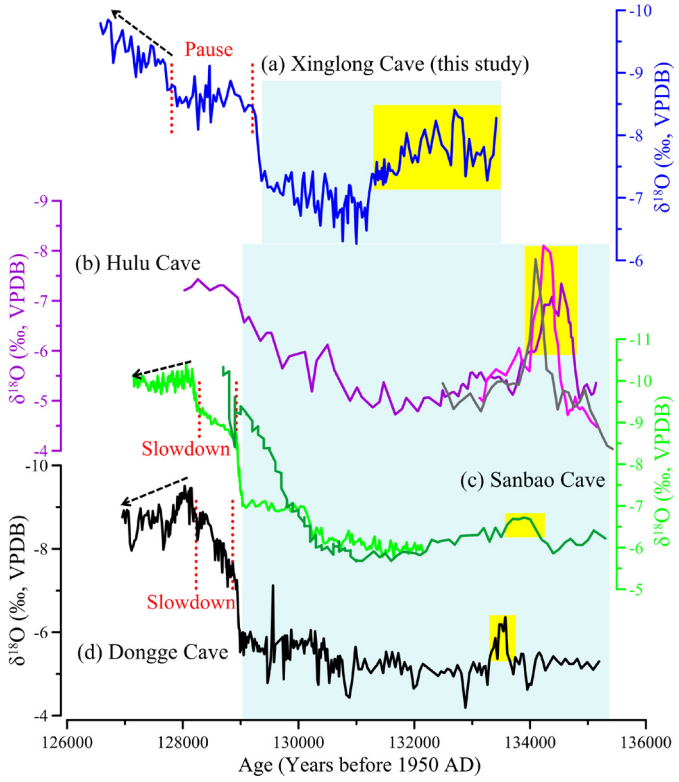

Fig. 3. Detailed structure of Termination II (T-II) identified in Chinese stalagmite $\delta^{18}O$ records. (a) XL-4 from Xinglong Cave (this study). (b) MSX (purple), MSP (magenta) and HLL162 (grey) from Hulu Cave (Cheng et al., 2006; Wang et al., 2018). (c) SB-11 (dark green) (Wang et al., 2008) and SB-25 (light green) (Cheng et al., 2009) from Sanbao Cave. (d) D4 from Dongge Cave (Kelly et al., 2006). Cyan and yellow vertical bars denote the "Weak Monsoon Interval" (WMI) and the interstadial within the WMI in each record, respectively. Red dash lines depict the climate "pause" or "slowdown" after the last interglacial onset. Black arrows depict the rough trend of $\delta^{18}O$ after the "pause" or "slowdown" phase.

5.2. The "Weak Monsoon Interval" (WMI) during T-II in China

A WMI (characterized by relatively high $\delta^{18}O$ values), several millennia in duration, immediately prior to the onset of the last interglacial, has been identified between 136 and 129 ka BP in south Chinese stalagmite records (Cheng et al., 2006, 2009; Kelly et al., 2006; Wang et al., 2018) (Figs. 3b, c, and d). Based on the close relationship between the WMI and episodes of ice-rafted debris (IRD) in the North Atlantic during T-I (Wang et al., 2001), the WMI during T-II (Cheng et al., 2006, 2009; Kelly et al., 2006) has previously been correlated to H11 recorded in the Ocean Drilling Program core (ODP) 980 (Fig. 4j) (McManus et al., 1999; Oppo et al., 2006) and the associated North Atlantic cold event (Martrat et al., 2014). Our data from north China also record this WMI characterized by relatively high $\delta^{18}O$ values before 129.4 ± 0.3 ka BP (Figs. 3a and 4d), which is mainly corresponding to the cold event H11.3 contained in H11 (Fig. 4k) (Tzedakis et al., 2018). Thus, the WMI recorded in the $\delta^{18}O$ of both north and south Chinese stalagmites corresponds to a decrease of northward surface-ocean heat transport, low North Atlantic sea-surface temperatures (Fig. 4b) (Jiménez-Amat and Zahn, 2015), and relatively high cave $\delta^{18}O$ values preceding the last interglacial onset in Israel (Fig. 4c) (Grant et al., 2012).

The mechanism behind these correlations was summarized by Cheng et al. (2006) as follows: the Northern Hemisphere summer insolation (NHSI) (Berger, 1978) was low but started to increase at around 136 ka BP (Fig. 4a), which triggered the initial retreat of northern ice sheets and resulted in major meltwater pulses into the North Atlantic (Figs. 4j and k) (Grant et al., 2014;

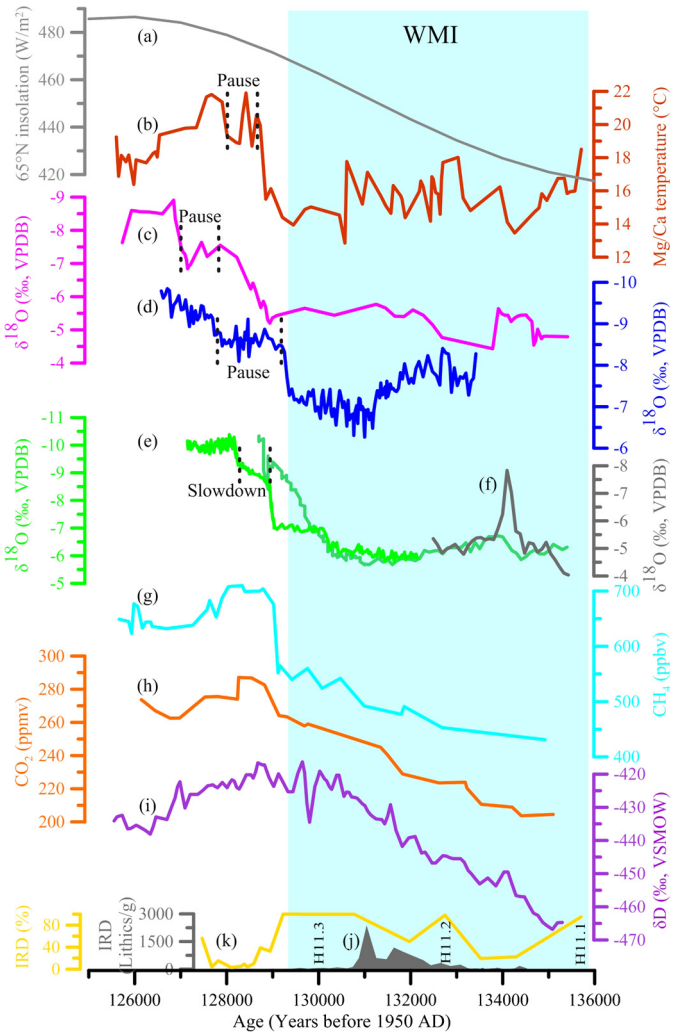

Fig. 4. Comparison of palaeoclimate records covering Termination II (T-II). (a) July insolation at 65°N (Berger, 1978). (b) The Ocean Drilling Program (ODP) core 976. *G. bulloides* Mg/Ca temperature (Jiménez-Amat and Zahn, 2015). (c) Soreq Cave (Bar-Matthews et al., 2003; Grant et al., 2012). (d) XL-4 from Xinglong Cave (this study). (e) SB-11 (dark green) and SB-25 (light green) (Cheng et al., 2009; Wang et al., 2008) from Sanbao Cave. (f) HL162 from Hulu Cave (Wang et al., 2018). (g) CH_4 concentration. (h) Atmospheric CO_2 concentration, and (i) δD records from Vostok (Petit et al., 1999) on the AICC2012 timescale (Bazin et al., 2013). (j) The ice-rafted debris (IRD) (Heinrich Event 11, H11) record from ODP 980 (Oppo et al., 2006) tuned to Sanbao Cave record (Cheng et al., 2009). (k) MD03-2664 IRD percentages (Irvalı et al., 2016) plotted on the Corchia Cave timescale (Tzedakis et al., 2018). H11.1, H11.2 and H11.3 denote the cold events contained in H11 (Tzedakis et al., 2018). The vertical cyan bar indicates the "Weak Monsoon Interval" (WMI) in Chinese cave records. Grey dash lines depict the climate "pause" or "slowdown" after the last interglacial onset.

Tzedakis et al., 2018). The influx of freshwater, in turn, induced a slow-down of the Atlantic Meridional Overturning Circulation (AMOC) (Tzedakis et al., 2018) and reduced the surface-ocean heat transport to the North Atlantic and resulted in lower winter temperatures. Associated with a greater extent of sea ice and enhanced snow cover, as well as the remaining ice sheets in northern Eurasia, this cold anomaly caused a southward shift of the Inter-tropical Convergence Zone (ITCZ) (Marino et al., 2015) and a weakening of the EASM (Zhang and Delworth, 2005). This interval, however, coincided with a warming in the Southern Hemisphere (Fig. 4i), resulting from the rise of atmospheric CO_2 (Fig. 4h) and CH_4 (Fig. 4g) (Petit et al., 1999) and a southward shift and/or possible strengthening of the Southern Ocean westerlies (Toggweiler et al., 2006). The asynchronous climate change between the hemispheres is consistent with the "bipolar seesaw" hypothesis (Marino et al., 2015).

5.3. The interstadial within the WMI during T-II

One of the most prominent features of our record is an (at least) 1600-year-long negative isotope excursion peaking at 132.7 ± 0.3 ka BP, immediately preceding the weakest phase of the WMI. The average $\delta^{18}O$ value of this interstadial is $-7.69‰$, much lighter than that of the following portion of the WMI ($-6.92‰$) (Fig. 3a). In south Chinese cave records, an interstadial within the WMI has been identified at around 134 ka BP, with a much smaller magnitude in the Dongge Cave and Sanbao Cave records than in the Hulu Cave records (Figs. 3b, c, d) (Cheng et al., 2006, 2009; Kelly et al., 2006; Wang et al., 2008, 2018). Cheng et al. (2009) argued that this interstadial is no more than several hundred years in length, and this may be so for the peak-interstadial monsoon strength, however, the negative excursion in the Sanbao Cave record persisted until ~132 ka BP (Fig. 3c) (Wang et al., 2008). Thus, the interstadial in the Sanbao Cave record is of comparative length to the (at least) 1600-year-long interstadial witnessed in the XL-4 record (Figs. 3a and c), although given the lack of the interstadial onset in XL-4 as well as the smaller magnitude in the Sanbao Cave record it is hard to be sure.

The interstadial at ~134 ka BP is also identified in some North Atlantic records, such as a short interruption in IRD with a concomitant decrease in *N. pachyderma* (*s*) abundance in ODP 984, south of Iceland (Mokeddem et al., 2014; Tzedakis et al., 2018) and also the rise in the alkenone-based SST in both ODP 976 from the Alboran basin (Martrat et al., 2014) and MD01-2444 on the Iberian Margin (Martrat et al., 2007, 2014; Tzedakis et al., 2018), however, all of which are too short to be the synchronous counterpart in XL-4. Nevertheless, the *G. bulloides* Mg/Ca-derived SST in ODP 976 shows a longer interstadial within H11 (Fig. 4b) than the alkenone SST in the same core (Jiménez-Amat and Zahn, 2015), and thus it may be related to that in XL-4 (Figs. 4b and d).

The millennial-scale interstadial within H11 observed in a few Chinese speleothem and North Atlantic records suggests that the main impact of the H11 freshwater pulse possibly occurred after 131.5 ka BP i.e. H11.3 (Tzedakis et al., 2018), and thus some aspects of ocean and atmospheric circulation remained in interstadial mode from 134 to 131.5 ka BP. This further suggests that it is reasonable to align the H11 peak to the high-$\delta^{18}O$ values in Chinese cave records at ~131.2 ka BP (Figs. 4j and 5i) (Cheng et al., 2009). Alternatively, it is also possible that the long and strong interstadial within the WMI in XL-4 is a more of a local event that is entirely unrelated to the North Atlantic. This needs to be checked by additional precisely dated records in the future.

5.4. The timing of the last interglacial onset

The most abrupt shift in the XL-4 $\delta^{18}O$ record with a decrease of 1.2‰ within 230 yr commenced at 129.4 ± 0.3 ka BP and marks the onset of the last interglacial (Figs. 3a, 4d and 5g). The timing of this abrupt transition is in excellent agreement with speleothem data from Sanbao Cave (Figs. 3c, 4e and 5h) (Cheng et al., 2009), Dongge Cave (Fig. 3d) (Kelly et al., 2006) and Hulu Cave (Fig. 3b) (Cheng et al., 2006) in south China and Xiaobailong Cave (Cai et al., 2015) in southwest China, Bittoo Cave in India (Kathayat et al., 2016), Clearwater Cave and Whiterock Cave in Borneo (Carolin et al., 2016). The synchronous timing of the last interglaial onset constrained by precise U–Th ages in north and south China as well as in the other Asian speleothem records further supports the idea that the NHSI plays an important role in initiating glacial terminations (Cheng et al., 2009).

The timing of the last interglacial onset archived in other mid- and low-latitudinal stalagmite records, such as Soreq Cave in Israel (Bar-Matthews et al., 2003; Grant et al., 2012) (Fig. 5f) and Sofular Cave in Turkey (Badertscher et al., 2011), is broadly coincident

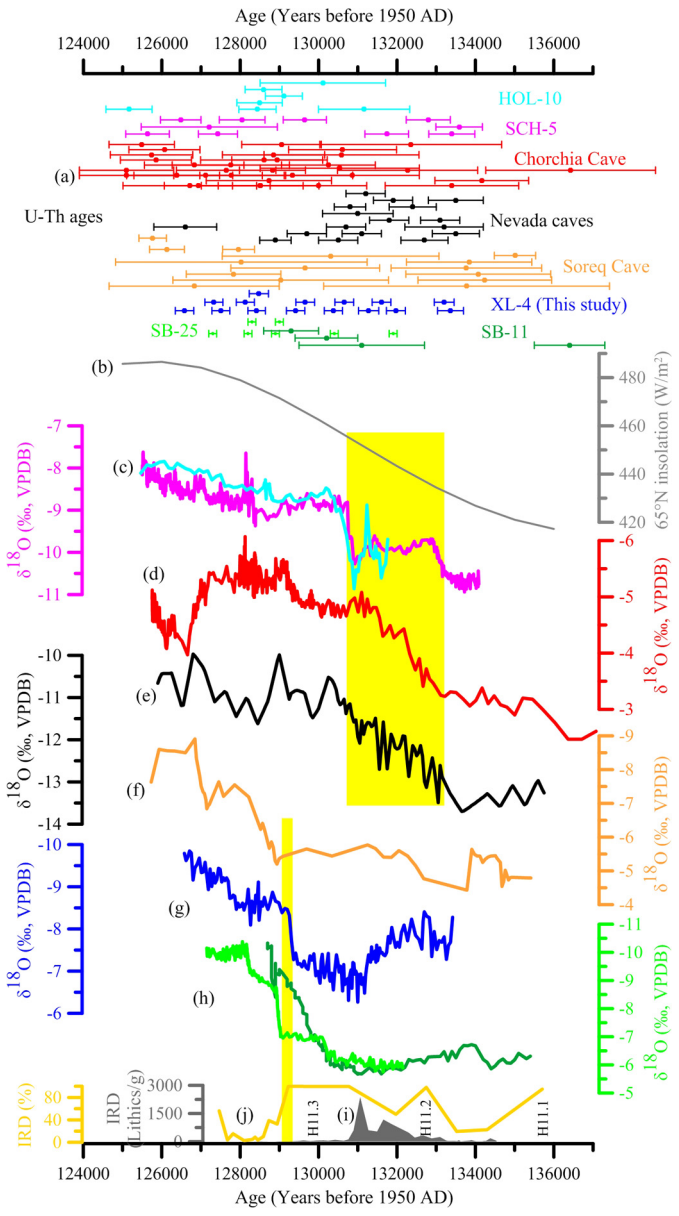

Fig. 5. The timing of the main $\delta^{18}O$ shift during Termination II (T-II) in different cave records. (a) U–Th ages with 2σ uncertainty for the stalagmtie records in this figure. Ages are color-coded by records. (b) July insolation at 65°N (Berger, 1978). (c) SCH-5 (magenta) and HOL-10 (cyan) from the European Alps caves (Moseley et al., 2015). (d) Corchia Cave stacked $\delta^{18}O$ (Tzedakis et al., 2018). (e) Composite of $\delta^{18}O$ from Nevada caves (Lachniet et al., 2014; Shakun et al., 2011). (f) Soreq Cave (Bar-Matthews et al., 2003; Grant et al., 2012). (g) XL-4 from Xinglong Cave (this study). (h) SB-11 (dark green) and SB-25 (light green) (Cheng et al., 2009; Wang et al., 2008) from Sanbao Cave. (i) The ice-rafted debris (IRD) (Heinrich Event 11, H11) record from the Ocean Drilling Program (ODP) 980 (Oppo et al., 2006) tuned to Sanbao Cave record (Cheng et al., 2009). (j) MD03-2664 IRD percentages (Irvalı et al., 2016) plotted on the Corchia Cave timescale (Tzedakis et al., 2018). H11.1, H11.2 and H11.3 denote the cold events contained in H11 (Tzedakis et al., 2018). The yellow vertical bars denote the main $\delta^{18}O$ shift in different records.

with the timing of the EASM shift (Fig. 5g and h). Whereas the main $\delta^{18}O$ shift documented in mid- and high-latitudinal stalagmite records started earlier, at around 132 ka BP, such as in Spannagel Cave (Spötl et al., 2007) and Schneckenloch Cave (Fig. 5c) (Moseley et al., 2015) in Austria, Corchia Cave (Fig. 5d) (Drysdale et al., 2009; Tzedakis et al., 2018) and Tan ache Urla Cave (Regattieri et al., 2014) in Italy, Schafsloch Cave (Häuselmann et al., 2015) in Switzerland, and Nevada caves (Fig. 5e) (Lachniet et al., 2014; Shakun et al., 2011) in North America.

Given the precise ^{230}Th dates of SCH-5, Nevada caves, XL-4 and SB-25, the apparent systematic age offset between these stalagmite records could be attributed to asynchronous climate change between mid-low-latitudinal and mid-high-latitudinal zones during T-II. However, if the substantial signals of the speleothem $\delta^{18}O$ records in the mid-high latitudes are closely inspected, the apparent earlier $\delta^{18}O$ shift at ~132 ka BP possibly reflects more local effects and not large-scale climate changes. The decrease in $\delta^{18}O$ at 133–132 ka BP in Corchia Cave, Italy, was attributed to changes in surface-hydrography in the North Atlantic associated with the meltwater penetration during H11.2 (Tzedakis et al., 2018) that was then transmitted via the hydrological cycle to the cave catchment (Drysdale et al., 2009; Tzedakis et al., 2018). The increase in $\delta^{18}O$ at ~132 ka BP in the other mid-high latitudinal speleothem records mentioned above may be related to the rising summer temperature associated with the increase of summer insolation (Häuselmann et al., 2015). For the alpine Schafsloch Cave record, alternatively, the basal glacial melting rather than the direct meteoric precipitation may be the reason of the earlier shift in $\delta^{18}O$. In the same vein, an inconsistency in the timing of the onset of the main shift during T-II was revealed by lacustrine and terrestrial proxies in a lake core in NW Greece where an abrupt shift to interglacial diatom assemblages (high lake level) occurred ~2700 yr prior to sustained forest expansion (peak precipitation). The earlier abrupt increase in lake level was attributed to the input of snow melt and glacial meltwater to the lake (Wilson et al., 2015). Additionally, a recent review of the global records around T-II suggested that although there is some evidence which suggests earlier deglacial increases in temperature and precipitation, the last interglacial onset in the North Atlantic and Europe occurred after the end of HS11 at ~129 ka BP (Govin et al., 2015).

In short, within age uncertainties, the abrupt resumption of the EASM coincides with the sharp North Atlantic SST increase (Fig. 4b) (Jiménez-Amat and Zahn, 2015; Oppo et al., 2006) as well as the drastic methane rise documented in Antarctic ice cores (Fig. 4g) (Petit et al., 1999), suggesting the synchronous rapid reestablishment of the global atmospheric and hydrological circulation pattern pointing to the onset of the last interglacial.

5.5. The climate change after the last interglacial onset

There is an obvious 1300-yr long "pause" centered at 128.4 ± 0.3 ka BP in the XL-4 $\delta^{18}O$ profile with oscillations between −9.1‰ and −8.1‰, immediately after the last interglacial onset (Fig. 3a), but only a "slowdown" in the rate of decrease in $\delta^{18}O$ in south Chinese speleothem records at this time interval (Figs. 3c and d) (Cheng et al., 2009; Kelly et al., 2006). An analogous climate "pause" after the last interstadial onset is also recorded in the $\delta^{18}O$ profile of Soreq Cave in Israel (Fig. 4c) (Bar-Matthews et al., 2003; Grant et al., 2012), and coincided with a decrease in SST recorded by Mg/Ca after the early peak warmth of the last interstadial by 3°C documented in ODP 976 (Fig. 4b) (Jiménez-Amat and Zahn, 2015). Additionally, there is a brief oscillation at the start of the last interglacial, the so-called cold event C28 in the North Atlantic at ~128.8 ka BP (Fig. 4k) as indicated by the $\delta^{13}C$ of *Cibicidoides wuellerstorfi* in core MD01-2444 on the Portuguese Margin on the new Corchia Cave timescale (Tzedakis et al., 2018), which might be coeval with the "pause/slowdown" in Chinese speleothems. Therefore, it is possible that the climate "pause" after the last interglacial onset is a large regional event, though the exact relationship between different records is still inconclusive. Nevertheless, this climate "pause" may not be termed as a YD-type event as its magnitude is much smaller than the YD during T-I. Previous researches (Carlson, 2008; Marino et al., 2015) suggested that during T-II compared to T-I, the ice sheets collapsed earlier and faster under stronger NHSI and higher atmosphere CO_2, and then more

meltwater was discharged to the North Atlantic. As a consequence, the AMOC was severely suppressed and was still not fully recovered even after the onset of the last interglacial. Thus, the pulses of freshwater after the last interglacial onset did not substantially decrease the relative weak AMOC, possibly explaining the occurring of a climate "pause" or "slowdown" but not a YD-type event.

After the "slowdown" phase, $\delta^{18}O$ in south Chinese speleothem records reached the minimum of the last interglacial at around 128 ka BP and then started to increase (Figs. 3c and d), whereas, after the climate "pause", XL-4 $\delta^{18}O$ values show a persistent decrease trend lasting until the end of the record at 126.6 ± 0.3 ka BP (Fig. 3a). This suggests the last interglacial peak of the EASM in north China may be later and stronger than in south China. Nevertheless, as XL-4 does not cover the full last interglacial, this argument should be confirmed by other longer records in the future.

The differences between XL-4 and south Chinese cave records after the last interglacial onset may be due to the location of Xinglong Cave near the northern boundary of the EASM region (Fig. S1), where precipitation is much more sensitive to the fluctuations of the EASM than in south China. In turn, even small changes in moisture trajectories and/or temperature could have a significant impact on $\delta^{18}O$ of precipitation.

6. Conclusions

A precisely dated stalagmite $\delta^{18}O$ record from Xinglong Cave documents the detailed evolution of T-II in north China for the first time, which mimics the main pattern of south Chinese cave records, especially the onset of the last interglacial at 129.4 ± 0.3 ka BP. These observations further support the NHSI as the initial trigger for glacial terminations. Nevertheless, before and after the last interglacial onset, the millennial-scale climate oscillations in our record are more remarkable than in south Chinese speleothem records, i.e. a stronger interstadial within the WMI and a climate "pause" after the last interglacial onset in north China vs. a weaker interstadial and a "slowdown" in south China. Possibly this is due to the location of Xinglong Cave, close to the northern boundary of the EASM, an area more sensitive to climate change than south China. However, the structure of T-II in our record is not an analogy of T-I, possibly because of the stronger North Hemisphere summer insolation, higher atmosphere CO_2, and the resultant faster and greater freshwater fluxes to the North Atlantic during T-II than during T-I.

Acknowledgements

We are grateful to Professor Andy Baker for his helpful comments and Dr. Youfeng Ning and Lijuan Sha for assistances with ^{230}Th dating and stable isotope measurements. We thank Jiuhua Geng, Yufen Li and Linan Ruan, the managers of Xinglong Cave, for their help in the field. Finally, we highly appreciate the constructive comments and suggestions of the journal editor Prof. Jess Adkins and the reviewer Prof. Christoph Spötl as well as the anonymous reviewers. This research was supported by the National Natural Science Foundation of China (Grant Nos. 41472150, 41772184, 41402164, 41731174 and 41888101), U.S. NSF Grant 1702816, and the International Postdoctoral Exchange Fellowship Program (Grant No. 20160093).

Author contributions

W.D. and M.T. designed the study and performed the fieldwork. H.C., W.D., X.L. and R.L.E. were responsible for ^{230}Th dating and W.D. for stable isotopic analyses. M.T. and W.D. collected the stalagmite sample. All authors contributed to the ideas in this manuscript. W.D. wrote the manuscript with contributions from all authors.

Competing financial interests

The authors declare no competing financial interests.

Appendix A. Supplementary material

All data of this study are included in the supplementary tables and any additional data can be obtained from W.D. (email: duanwuhui@mail.iggcas.ac.cn). Supplementary material related to this article can be found online at https://doi.org/10.1016/j.epsl.2019.01.043.

References

Badertscher, S., Fleitmann, D., Cheng, H., Edwards, R.L., Göktürk, O.M., Zumbühl, A., Leuenberger, M., Tuysuz, O., 2011. Pleistocene water intrusions from the Mediterranean and Caspian seas into the Black Sea. Nat. Geosci. 4, 236–239.

Baker, A., Asrat, A., Fairchild, I.J., Leng, M.J., Wynn, P.M., Bryant, C., Genty, D., Umer, M., 2007. Analysis of the climate signal contained within $\delta^{18}O$ and growth rate parameters in two Ethiopian stalagmites. Geochim. Cosmochim. Acta 71, 2975–2988.

Bar-Matthews, M., Ayalon, A., Gilmour, M., Matthews, A., Hawkesworth, C.J., 2003. Sea-land oxygen isotopic relationships from planktonic foraminifera and speleothems in the Eastern Mediterranean region and their implication for paleorainfall during interglacial intervals. Geochim. Cosmochim. Acta 67, 3181–3199.

Bauch, H.A., Kandiano, E.S., Helmke, J.P., 2012. Contrasting ocean changes between the subpolar and polar North Atlantic during the past 135 ka. Geophys. Res. Lett. 39, L11604.

Bazin, L., Landais, A., Lemieux-Dudon, B., Toyé Mahamadou Kele, H., Veres, D., Parrenin, F., Martinerie, P., Ritz, C., Capron, E., Lipenkov, V., Loutre, M.F., Raynaud, D., Vinther, B., Svensson, A., Rasmussen, S.O., Severi, M., Blunier, T., Leuenberger, M., Fischer, H., Masson-Delmotte, V., Chappellaz, J., Wolff, E., 2013. An optimized multi-proxy, multi-site Antarctic ice and gas orbital chronology (AICC2012): 120–800 ka. Clim. Past 9, 1715–1731.

Berger, A., 1978. Long-term variations of caloric insolation resulting from the earth's orbital elements. Quat. Res. 9, 139–167.

Cai, Y., Fung, I.Y., Edwards, R.L., An, Z., Cheng, H., Lee, J.-E., Tan, L., Shen, C.-C., Wang, X., Day, J.A., Zhou, W., Kelly, M.J., Chiang, J.C.H., 2015. Variability of stalagmite-inferred Indian monsoon precipitation over the past 252,000 y. Proc. Natl. Acad. Sci. USA 112, 2954–2959.

Carlson, A.E., 2008. Why there was not a Younger Dryas-like event during the Penultimate Deglaciation. Quat. Sci. Rev. 27, 882–887.

Carolin, S.A., Cobb, K.M., Lynch-Stieglitz, J., Moerman, J.W., Partin, J.W., Lejau, S., Malang, J., Clark, B., Tuen, A.A., Adkins, J.F., 2016. Northern Borneo stalagmite records reveal West Pacific hydroclimate across MIS 5 and 6. Earth Planet. Sci. Lett. 439, 182–193.

Cheng, H., Edwards, R.L., Broecker, W.S., Denton, G.H., Kong, X., Wang, Y., Zhang, R., Wang, X., 2009. Ice age terminations. Science 326, 248–252.

Cheng, H., Edwards, R.L., Wang, Y., Kong, X., Ming, Y., Kelly, M.J., Wang, X., Gallup, C.D., Liu, W., 2006. A penultimate glacial monsoon record from Hulu Cave and two-phase glacial terminations. Geology 34, 217–220.

Cheng, H., Lawrence Edwards, R., Shen, C.-C., Polyak, V.J., Asmerom, Y., Woodhead, J., Hellstrom, J., Wang, Y., Kong, X., Spötl, C., Wang, X., Calvin Alexander Jr., E., 2013. Improvements in ^{230}Th dating, ^{230}Th and ^{234}U half-life values, and U–Th isotopic measurements by multi-collector inductively coupled plasma mass spectrometry. Earth Planet. Sci. Lett. 371–372, 82–91.

Clemens, S.C., Prell, W.L., Sun, Y., 2010. Orbital-scale timing and mechanisms driving Late Pleistocene Indo-Asian summer monsoons: reinterpreting cave speleothem $\delta^{18}O$. Paleoceanography 25, PA4207.

Drysdale, R.N., Hellstrom, J.C., Zanchetta, G., Fallick, A.E., Sánchez Goñi, M.F., Couchoud, I., McDonald, J., Maas, R., Lohmann, G., Isola, I., 2009. Evidence for obliquity forcing of glacial Termination II. Science 325, 1527–1531.

Duan, W., Cheng, H., Tan, M., Edwards, R.L., 2016a. Onset and duration of transitions into Greenland Interstadials 15.2 and 14 in northern China constrained by an annually laminated stalagmite. Sci. Rep. 6, 20844.

Duan, W., Ruan, J., Luo, W., Li, T., Tian, L., Zeng, G., Zhang, D., Bai, Y., Li, J., Tao, T., Zhang, P., Baker, A., Tan, M., 2016b. The transfer of seasonal isotopic variability between precipitation and drip water at eight caves in the monsoon regions of China. Geochim. Cosmochim. Acta 183, 250–266.

Dykoski, C.A., Edwards, R.L., Cheng, H., Yuan, D., Cai, Y., Zhang, M., Lin, Y., Qing, J., An, Z., Revenaugh, J., 2005. A high-resolution, absolute-dated Holocene and deglacial Asian monsoon record from Dongge Cave, China. Earth Planet. Sci. Lett. 233, 71–86.

Edwards, R.L., Chen, J.H., Wasserburg, G.J., 1987. ^{238}U–^{234}U–^{230}Th–^{232}Th systematics and the precise measurement of time over the past 500,000 years. Earth Planet. Sci. Lett. 81, 175–192.

Friedman, I., O'Neil, J.R., 1977. Compilation of stable isotopefractionation factors of geochemical interest. In: Fleisher, M. (Ed.), Data of Geochemistry, 6th ed. U.S. Geological Survey Professional Paper 440-KK, 12 p.

Govin, A., Capron, E., Tzedakis, P.C., Verheyden, S., Ghaleb, B., Hillaire-Marcel, C., St-Onge, G., Stoner, J.S., Bassinot, F., Bazin, L., Blunier, T., Combourieu-Nebout, N., El Ouahabi, A., Genty, D., Gersonde, R., Jimenez-Amat, P., Landais, A., Martrat, B., Masson-Delmotte, V., Parrenin, F., Seidenkrantz, M.S., Veres, D., Waelbroeck, C., Zahn, R., 2015. Sequence of events from the onset to the demise of the Last Interglacial: evaluating strengths and limitations of chronologies used in climatic archives. Quat. Sci. Rev. 129, 1–36.

Grant, K.M., Rohling, E.J., Bar-Matthews, M., Ayalon, A., Medina-Elizalde, M., Ramsey, C.B., Satow, C., Roberts, A.P., 2012. Rapid coupling between ice volume and polar temperature over the past 150,000 years. Nature 491, 744–747.

Grant, K.M., Rohling, E.J., Ramsey, C.B., Cheng, H., Edwards, R.L., Florindo, F., Heslop, D., Marra, F., Roberts, A.P., Tamisiea, M.E., Williams, F., 2014. Sea-level variability over five glacial cycles. Nat. Commun. 5, 5076.

Häuselmann, A.D., Fleitmann, D., Cheng, H., Tabersky, D., Günther, D., Edwards, R.L., 2015. Timing and nature of the penultimate deglaciation in a high alpine stalagmite from Switzerland. Quat. Sci. Rev. 126, 264–275.

Hendy, C.H., 1971. The isotopic geochemistry of speleothems, I: the calculation of the effects of different modes of formation on the isotopic composition of speleothems and their applicability as palaeoclimatic indicators. Geochim. Cosmochim. Acta 35, 801–824.

Irvalı, N., Ninnemann, U.S., Kleiven, H.F., Galaasen, E.V., Morley, A., Rosenthal, Y., 2016. Evidence for regional cooling, frontal advances, and East Greenland Ice Sheet changes during the demise of the last interglacial. Quat. Sci. Rev. 150, 184–199.

Jiménez-Amat, P., Zahn, R., 2015. Offset timing of climate oscillations during the last two glacial–interglacial transitions connected with large-scale freshwater perturbation. Paleoceanography 30, 768–788.

Kathayat, G., Cheng, H., Sinha, A., Spötl, C., Edwards, R.L., Zhang, H., Li, X., Yi, L., Ning, Y., Cai, Y., Lui, W.L., Breitenbach, S.F.M., 2016. Indian monsoon variability on millennial-orbital timescales. Sci. Rep. 6, 24374.

Kelly, M.J., Edwards, R.L., Cheng, H., Yuan, D., Cai, Y., Zhang, M., Lin, Y., An, Z., 2006. High resolution characterization of the Asian Monsoon between 146,000 and 99,000 years B.P. from Dongge Cave, China and global correlation of events surrounding Termination II. Palaeogeogr. Palaeoclimatol. Palaeoecol. 236, 20–38.

Lachniet, M.S., Denniston, R.F., Asmerom, Y., Polyak, V.J., 2014. Orbital control of western North America atmospheric circulation and climate over two glacial cycles. Nat. Commun. 5, 3805.

Liu, D., Wang, Y., Cheng, H., Lawrence Edwards, R., Kong, X., Wang, X., Hardt, B., Wu, J., Chen, S., Jiang, X., 2010. Sub-millennial variability of Asian monsoon intensity during the early MIS 3 and its analogue to the ice age terminations. Quat. Sci. Rev. 29, 1107–1115.

Liu, Z., Wen, X., Brady, E.C., Otto-Bliesner, B., Yu, G., Lu, H., Cheng, H., Wang, Y., Zheng, W., Ding, Y., Edwards, R.L., Cheng, J., Liu, W., Yang, H., 2014. Chinese cave records and the East Asia Summer Monsoon. Quat. Sci. Rev. 83, 115–128.

Ma, Z.B., Cheng, H., Tan, M., Edwards, R.L., Li, H.C., You, C.F., Duan, W.H., Wang, X., Kelly, M.J., 2012. Timing and structure of the Younger Dryas event in northern China. Quat. Sci. Rev. 41, 83–93.

Marino, G., Rohling, E.J., Rodriguez-Sanz, L., Grant, K.M., Heslop, D., Roberts, A.P., Stanford, J.D., Yu, J., 2015. Bipolar seesaw control on last interglacial sea level. Nature 522, 197–201.

Martrat, B., Grimalt, J.O., Shackleton, N.J., de Abreu, L., Hutterli, M.A., Stocker, T.F., 2007. Four climate cycles of recurring deep and surface water destabilizations on the Iberian Margin. Science 317, 502–507.

Martrat, B., Jimenez-Amat, P., Zahn, R., Grimalt, J.O., 2014. Similarities and dissimilarities between the last two deglaciations and interglaciations in the North Atlantic region. Quat. Sci. Rev. 99, 122–134.

McManus, J.F., Oppo, D.W., Cullen, J.L., 1999. A 0.5-million-year record of millennial-scale climate variability in the North Atlantic. Science 283, 971–975.

Mokeddem, Z., McManus, J.F., Oppo, D.W., 2014. Oceanographic dynamics and the end of the last interglacial in the subpolar North Atlantic. Proc. Natl. Acad. Sci. USA 111, 11263–11268.

Moseley, G.E., Spötl, C., Cheng, H., Boch, R., Min, A., Edwards, R.L., 2015. Termination-II interstadial/stadial climate change recorded in two stalagmites from the north European Alps. Quat. Sci. Rev. 127, 229–239.

Oppo, D.W., McManus, J.F., Cullen, J.L., 2006. Evolution and demise of the Last Interglacial warmth in the subpolar North Atlantic. Quat. Sci. Rev. 25, 3268–3277.

Pausata, F.S., Battisti, D.S., Nisancioglu, K.H., Bitz, C.M., 2011. Chinese stalagmite $\delta^{18}O$ controlled by changes in the Indian monsoon during a simulated Heinrich event. Nat. Geosci. 4, 474–480.

Petit, J.R., Jouzel, J., Raynaud, D., Barkov, N.I., Barnola, J.M., Basile, I., Bender, M., Chappellaz, J., Davis, M., Delaygue, G., Delmotte, M., Kotlyakov, V.M., Legrand, M., Lipenkov, V.Y., Lorius, C., Pepin, L., Ritz, C., Saltzman, E., Stievenard, M., 1999. Climate and atmospheric history of the past 420,000 years from the Vostok ice core, Antarctica. Nature 399, 429–436.

Regattieri, E., Zanchetta, G., Drysdale, R.N., Isola, I., Hellstrom, J.C., Roncioni, A., 2014. A continuous stable isotope record from the penultimate glacial maximum to the Last Interglacial (159–121 ka) from Tana Che Urla Cave (Apuan Alps, central Italy). Quat. Res. 82, 450–461.

Scholz, D., Hoffmann, D.L., 2011. StalAge – an algorithm designed for construction of speleothem age models. Quat. Geochronol. 6, 369–382.

Shakun, J.D., Burns, S.J., Clark, P.U., Cheng, H., Edwards, R.L., 2011. Milankovitch-paced Termination II in a Nevada speleothem? Geophys. Res. Lett. 38, L18701.

Spötl, C., Holzkämper, S., Mangini, A., 2007. The last and the penultimate interglacial as recorded by speleothems from a climatically sensitive high-elevation cave site in the Alps. In: Sirocko, F., Claussen, M., Sánchez Goñi, M.F., Litt, T. (Eds.), Developments in Quaternary Sciences, vol. 7, pp. 471–491.

Tan, M., 2014. Circulation effect: response of precipitation $\delta^{18}O$ to the ENSO cycle in monsoon regions of China. Clim. Dyn. 42, 1067–1077.

Toggweiler, J.R., Russell, J.L., Carson, S.R., 2006. Midlatitude westerlies, atmospheric CO_2, and climate change during the ice ages. Paleoceanography 21, PA2005.

Tzedakis, P.C., Drysdale, R.N., Margari, V., Skinner, L.C., Menviel, L., Rhodes, R.H., Taschetto, A.S., Hodell, D.A., Crowhurst, S.J., Hellstrom, J.C., Fallick, A.E., Grimalt, J.O., McManus, J.F., Martrat, B., Mokeddem, Z., Parrenin, F., Regattieri, E., Roe, K., Zanchetta, G., 2018. Enhanced climate instability in the North Atlantic and southern Europe during the Last Interglacial. Nat. Commun. 9, 4235.

Wang, Q., Wang, Y., Shao, Q., Liang, Y., Zhang, Z., Kong, X., 2018. Millennial-scale Asian monsoon variability during the late Marine Isotope Stage 6 from Hulu Cave, China. Quat. Res. 90, 394–405.

Wang, Y., Cheng, H., Edwards, R.L., Kong, X., Shao, X., Chen, S., Wu, J., Jiang, X., Wang, X., An, Z., 2008. Millennial- and orbital-scale changes in the East Asian monsoon over the past 224,000 years. Nature 451, 1090–1093.

Wang, Y.J., Cheng, H., Edwards, R.L., An, Z.S., Wu, J.Y., Shen, C.C., Dorale, J.A., 2001. A high-resolution absolute-dated late Pleistocene monsoon record from Hulu Cave, China. Science 294, 2345–2348.

Wilson, G.P., Reed, J.M., Frogley, M.R., Hughes, P.D., Tzedakis, P.C., 2015. Reconciling diverse lacustrine and terrestrial system response to penultimate deglacial warming in southern Europe. Geology 43, 819–822.

Zhang, R., Delworth, T.L., 2005. Simulated tropical response to a substantial weakening of the Atlantic thermohaline circulation. J. Climate 18, 1853–1860.